Electronic Supplementary Material (ESI) for ChemComm.

3d-4f heterometallic cluster incorporated polyoxoniobates with magnetic property

Yu-Diao Lin,[a] Rui Ge,[a] Chong-Bin Tian,[b] Cai Sun,[a] Yan-Qiong Sun,[a] Qing-Xin Zeng,*[a], Xin-Xiong Li,*[a,b] Shou-Tian Zheng[a]

[a] *State Key Laboratory of Photocatalysis on Energy and Environment, College of Chemistry, Fuzhou University, Fuzhou, Fujian 350108, China.*

[b] *State Key Laboratory of Structural Chemistry, Fujian Institute of Research on the Structure of Matter, Chinese Academy of Sciences, Fuzhou, Fujian 350002, China.*

E-mail: *T04007@fzu.edu.cn*; *lxx@fzu.edu.cn*,

This file includes:

Section S1: Experiments and Methods

1. Materials and General methods:

All chemical materials were commercially purchased without further purification. Infrared (IR) spectra (KBr pellet) were performed on an Opus Vetex 70 FT-IR infrared spectrophotometer in the range of 400-4000 cm^{-1} (Fig. S7). Powder X-ray diffraction (PXRD) patterns were recorded on a Rigaku DMAX 2500 diffractometer with CuKα radiation (λ = 1.54056 Å). Simulated XRD data were simulated by the Mercury Software with the step of 0.02° from 5° to 50°. Thermogravimetric analyses were conducted using a Mettler Toledo TGA/SDTA 851^e analyzer in an N_2-flow atmosphere with a heating rate of 10 °C/min at a temperature of 25-800 °C. Variable temperature susceptibility measurements were carried out in the temperature range of 2-300 K at a magnetic field of 0.1 T on polycrystalline samples with a Quantum Design PPMS-9T magnetometer. The experimental susceptibilities were corrected for the Pascal's constants. UV-vis spectra were performed on a SHIMADZU UV-2600 UV-visible spectrophotometer by using the $BaSO_4$ as the blank.

2. Syntheses

Synthesis of 1-Cr-Dy: A mixture of $K_7HNb_6O_{19}\cdot13H_2O$(0.27 mmol, 373 mg), $Dy(NO_3)_3\cdot6H_2O$ (0.14 mmol, 65 mg), $CrCl_3\cdot6H_2O$ (0.24 mmol, 65 mg) Tris (hydroxymethyl aminomethane) (0.53 mmol, 65 mg), and 8 ml $Na_2CO_3/NaHCO_3$ buffer solution (0.05 M, pH = 10.5) was stirred in a 20 mL vial, and then heated at 90 °C for 3 days. After cooling down, the filtrate was kept at room temperature for two weeks and green hexagonal prisms crystals of **1-Cr-Dy** suitable for X-ray diffraction experiments were obtained. Yield: 16.21% (based on $K_7HNb_6O_{19}\cdot13H_2O$). IR (KBr, cm^{-1}): 3289(s), 1635(m), 1586(w), 1581(w), 1367(m), 1034(w), 857(s), 647(s) 508(m).

Synthesis of 1-Mn-Dy: 1-Mn-Dy was prepared by a procedure similar to that of **1-Cr-Dy**, except for the replacement of $CrCl_3\cdot6H_2O$ by $MnCl_2\cdot4H_2O$ (0.33 mmol, 65 mg). Yield: about 17 % (based on $K_7HNb_6O_{19}\cdot13H_2O$). IR (KBr, cm^{-1}): 3182(s), 1639(m), 1371(s), 845(s), 643(s), 512(s).

Synthesis of 1-Fe-Dy: 1-Fe-Dy was prepared by a procedure similar to that of **1-Cr-Dy**, except for the replacement of $CrCl_3\cdot6H_2O$ by $FeSO_4\cdot7H_2O$ (0.23 mmol, 65 mg). Yield: about 67 % (based on $K_7HNb_6O_{19}\cdot13H_2O$). IR (KBr, cm^{-1}): 3194(s), 1643(m), 1375(m), 845(s), 656(s), 516(m).

Synthesis of 1-Co-Dy: 1-Co-Dy was prepared by a procedure similar to that of **1-Cr-Dy**, except for the replacement of $CrCl_3\cdot6H_2O$ by $CoCl_2\cdot6H_2O$ (0.27mmol, 65 mg). Yield: about 67 % (based on $K_7HNb_6O_{19}\cdot13H_2O$). IR (KBr, cm^{-1}): 3198(s), 1643(w) 1367(m), 845(s), 647(s), 520(s).

3. Single-crystal structure analyses

Single-crystal X-ray diffraction data of **1-TM-Dy** was collected on Bruker Apex Duo CCD differactometer with a graphite-monochromatized (Mo Kα radiation, λ = 0.71073 Å) operation at 175 K. The structures of **1-TM-Dy** were solved by a direct method followed by successive different Fourier methods, and were refined by full-matrix least-squares refinements based on F^2 using the SHELX-2013-2 package. Calculations were done using SHELXTL and were refined by final full-matrix least-squares refinements against F^2. The contribution of solvents to the overall intensity data of

structures was removed by using the SQUEEZE method in PLATON. The final formulas of **1-TM-Dy** were determined by using single-crystal X-ray diffraction combined with thermogravimetric analysis (Fig. S8). Crystallographic data and structure refinements for **1-TM-Dy** are summarized in Table S1. CCDC 2088428, 2088429, 2088430, and 2088431 contain supplementary crystallographic data for this paper. These data can be obtained free of charge from The Cambridge Crystallographic Data Centre via www.ccdc.cam.ac.uk/data_request/cif.

3. Synthesis Discussion

In this work, we found that the combination of the hydrothermal reaction and the slow evaporation is a particularly powerful and suitable strategy for **1-TM-Dy**. Besides, the following reaction parameters also show important impacts on the syntheses:

(1) The syntheses of **1-TM-Dy** are highly sensitive to transition metals and their valence. Only those metals that have the +3 oxidation state such as Cr, Mn, Fe, and Co can form the product. Besides, for **1-Mn-Dy/1-Fe-Dy/1-Co-Dy**, using divalent TM salts as the starting materials is more appropriate to grow the crystals. If trivalent metal ions (Mn^{III}, Fe^{III}, and Co^{III}) were directly introduced, no crystals could be obtained. The final trivalent metal species in the crystals were generated by in situ oxidation of the divalent salts during the hydrothermal reaction and slow evaporation processes.[S1] In addition, the yields of **1-Cr-Dy** and **1-Mn-Dy** are lower than those of **1-Fe-Dy** and **1-Co-Dy**, probably because 1) the reductive Cr^{III} ion is easy to be oxidized in a basic condition; 2) the Mn^{III} ion is unstable in solution and prone to disproportionation; 3) the Co^{III} and Fe^{III} ions are relatively stable in an oxidizing condition.

(2) The syntheses of **1-TM-Dy** are also sensitive to lanthanide ions. When the light lanthanide metals such as La, Ce, Pr, Nd, and Sm were used as the starting materials, only amorphous precipitation instead of crystals could be obtained.

(3) Na_2CO_3/$NaHCO_3$ buffer solution is crucial to the syntheses of these compounds since the buffer solution can maintain the pH value of the reaction system in a reasonable range. Moreover, Na_2CO_3 and $NaHCO_3$ can act as mineralizers that are in favor of the crystallization of PONbs.

(4) Tris is an important additive for the formation of compounds, though it is not present in the final products. Tris is a weak base that can finely adjust the pH value of the reaction system and maintain it in an appropriate range. What's more, Tris can protect TM and Ln ions from being hydrolyzed into insoluble precipitation under basic conditions through the coordination interactions between metal ions and the three hydroxyl groups. During the slow evaporation, TM and Ln ions would be slowly released to take part in the crystallization process.

(5) The temperature of the initial hydrothermal reactions also plays a vital role in the formation of **1-TM-Dy**. When the reaction temperature is higher than 110°C or lower than 70°C, the yield would decrease dramatically and only amorphous phases would be obtained.

Section S2 Additional Tables

Table S1 Crystallographic data of 1-TM-Dy

Compound	**1-Cr-Dy**	**1-Mn-Dy**	**1-Fe-Dy**	**1-Co-Dy**
Empirical formula	$H_{144}Cr_2Dy_6Na_6$ $Nb_{30}O_{210}$	$H_{146}Dy_6Mn_2Na_6$ $Nb_{30}O_{211}$	$H_{146}Dy_6Fe_2Na_6$ $Nb_{30}O_{214}$	$H_{132}Co_2Dy_6Na_6$ $Nb_{30}O_{197}$
Formula weight	7496.24	7503.12	7561.94	7295.34
Crystal system	trigonal	trigonal	trigonal	trigonal
Space group	$P\bar{3}1c$	$P\bar{3}1c$	$P\bar{3}1c$	$P\bar{3}1c$
a (Å)	18.9817(6)	19.0042(7)	18.9931(3)	19.0037(3)
b (Å)	18.9817(6)	19.0042(7)	18.9931(3)	19.0037(3)
c (Å)	28.8986(15)	28.9507(17)	29.0291(7)	28.6076(11)
α	90	90	90	90
β	90	90	90	90
γ	120	120	120	120
V (Å^3)	9017.3(7)	9055.0(9)	9068.9(4)	8947.2(4)
Z	2	2	2	2
F(000)	5848	5852	5904	5748
Temperature (K)	175(2)	175(2)	175(2)	175(2)
σ (g/cm^3)	2.347	2.339	2.354	2.329
μ(mm^{-1})	4.507	4.502	4.518	4.596
Reflns Collected /unique restraints / Parameters	5334 / 12 / 281	5316 / 12 / 281	5366 / 12 / 278	5194 / 12 / 281
Completeness	97.5 %	96.7 %	97.6 %	95.8 %
GOF on F^2	0.857	0.824	0.876	1.072
Final *R* indices	R_1 = 0.0343	R_1 = 0.0305	R_1 = 0.0361	R_1 = 0.0353
(I= 2σ(I))	wR_2 = 0.1018	wR_2 = 0.0775	wR_2 = 0.1090	wR_2 =0.0783
R indices	R_1 = 0.0419	R_1 = 0.0366	R_1 = 0.0456	R_1 = 0.0416
(all data)	wR_2 = 0.1078	wR_2 = 0.0811	wR_2 = 0.1128	wR_2 = 0.0811

$R_1{}^a = \sum||F_o| - |F_c||/\sum|F_o|$. $wR_2 = [\sum w(F_o{}^2 - F_c{}^2)^2/\sum w(F_o{}^2)^2]^{1/2}$, x = 0.0814, y = 56.1758 for **1-Cr-Dy**; x = 0.0489, y = 87.9080 for **1-Mn-Dy**; X = 0.0675, y = 24.5532 for **1-Fe-Dy**; x = 0.0301, y = 66.538506 for **1-Co-Dy**.

Table S2 Selected band length (Å) and valence band summations (Σ_s) for 1-TM-Dy

1-Cr-Dy			
Bond	Bond length (Å)	Bond valence	Sum of Bond
Cr1-O6	1.963	0.523	Σ_S=3.10
Cr1-O6	1.963	0.523	

Cr1-O6	1.963	0.523	
Cr1-O5	1.972	0.523	
Cr1-O5	1.972	0.523	
Cr1-O5	1.972	0.523	
Dy1-O2	2.262	0.535	
Dy1-O4	2.332	0.434	
Dy1-O5	2.370	0.388	
Dy1-O8	2.409	0.345	
Dy1-O3	2.415	0.339	Σ_S=3.00
Dy1-O7	2.418	0.335	
Dy1-O1	2.437	0.317	
Dy1-O5	2.445	0.310	
1-Mn-Dy			
Bond	Bond length (Å)	Bond valence	Sum of Bond
Mn1-O18	1.967	0.571	
Mn1-O18	1.967	0.571	
Mn1-O18	1.967	0.571	
Mn1-O7	1.985	0.544	Σ_S=3.34
Mn1-O7	1.985	0.544	
Mn1-O7	1.985	0.544	
Dy1-O2	2.262	0.498	
Dy1-O3	2.324	0.413	
Dy1-O5	2.373	0.357	
Dy1-O4	2.405	0.324	
Dy1-O6	2.409	0.321	Σ_S=3.14
Dy1-O7	2.424	0.307	
Dy1-O1	2.436	0.296	
Dy1-O5	2.459	0.277	
1-Fe-Dy			
Bond	Bond length (Å)	Bond valence	Sum of Bond
Fe1-O7	1.999	0.522	
Fe1-O7	1.999	0.522	
Fe1-O7	1.999	0.522	
Fe1-O6	2.006	0.512	Σ_S=3.12
Fe1-O6	2.006	0.512	
Fe1-O6	2.006	0.512	
Dy1-O3	2.263	0.541	
Dy1-O2	2.327	0.454	
Dy1-O6	2.379	0.395	
Dy1-O4	2.406	0.367	Σ_S=3.12
Dy1-O10	2.410	0.363	
Dy1-O9	2.430	0.344	
Dy1-O1	2.437	0.337	

Dy1-O6	2.458	0.319	
1-Co-Dy			
Bond	Bond length (Å)	Bond valence	Sum of Bond
Co1-O4	1.903	0.554	Σ_S=3.29
Co1-O4	1.903	0.554	
Co1-O4	1.903	0.554	
Co1-O7	1.911	0.543	
Co1-O7	1.911	0.543	
Co1-O7	1.911	0.543	
Dy1-O3	2.257	0.565	Σ_S=3.17
Dy1-O2	2.321	0.434	
Dy1-O4	2.371	0.388	
Dy1-O10	2.417	0.345	
Dy1-O9	2.413	0.339	
Dy1-O8	2.419	0.335	
Dy1-O4	2.425	0.317	
Dy1-O1	2.440	0.310	

Table S3 The caculation of the energy barrier (E_a/k_B) of 1-TM-Dy

1-Cr-Dy		
Frequency (Hz)	Slope	E_a/k_B
311	0.998	0.998
511	1.119	1.119
711	1.350	1.350
911	1.285	1.285
1311	1.319	1.319
1711	1.951	1.951
2111	1.623	1.623
1-Mn-Dy		
Frequency (Hz)	Slope	E_a/k_B
311	4.995	4.995
511	4.466	4.466
711	4.099	4.099
911	3.807	3.807
1311	3.375	3.375
1711	3.006	3.006
2111	2.824	2.824
1-Fe-Dy		
Frequency (Hz)	Slope	E_a/k_B
311	3.851	3.851
511	2.948	2.948
711	2.280	2.280

911	1.693	1.693
1311	2.184	2.184
1711	1.643	1.643
2111	1.769	1.769
1-Co-Dy		
Frequency (Hz)	Slope	E_a/k_B
311	3.012	3.012
511	2.274	2.274
711	2.389	2.389
911	2.495	2.495
1311	2.477	2.477
1711	2.435	2.435
2111	2.303	2.303

As shown in Table S3, the energy barrier of **1-TM-Dy** does not have an obvious trend. **1-Mn-Dy** presents the highest energy barrier than other compounds. So far, the calculation of energy barrier has not been found in the reported 3d-4f heterometallic cluster incorporated POMs. But, the energy barrier of **1-TM-Dy** is lower than that of the most 3d-4f heterometallic complexes (Table S4). For **1-TM-Dy**, Cr^{III} is a paramagnetic ion, while Co^{III} (d^6 electronic configuration, S = 0) is a diamagnetic ion. The introduction of paramagnetic Cr^{III} (d^3 electronic configuration, S = 3/2) was supposed to increase the energy barrier,[S2] but, due to the magnetic dipole-dipole interaction, the introduction of Cr^{III} may have a negative effect on the anisotropy of Dy^{III}, the energy barrier of **1-Cr-Dy** is smaller than **1-Co-Dy;** Mn^{III} (d^4 electronic configuration, S = 2) is an important ion for slow relaxation behavior and often result in a negative zero-field splitting parameter as desired for single-molecule magnetism;[S3] Paramagnetic high spin Fe^{III} (d^5 electronic configuration, S = 5/2) is isotropic and may provide a strong antiferromagnetic exchange with other Fe^{III} and most of the cases give small or zero ground state spins.[S4] Thus, different 3d ions may have different effects on the electron density of the coordination atoms and the crystal field of 4f ions, and they mainly affect the magnetic anisotropy of Dy^{III}. Moreover, the magnetic dipole-dipole interaction between the 3d and 4f metal ions may also have a certain effect on the energy barrier.[S5]

Table S4 The energy barrier of some reported 3d-4f heterometallic compounds

3d-4f compounds	**Energy barrier (E_a/k_B)**	**Ref**
$[Cr^{III}_4Dy^{III}_4(\mu_3\text{-}OH)_4(\mu\text{-}N_3)_4(mdea)_4(piv)_4]_3CH_2Cl_2$	15	S6
$[Mn^{III}_6Tb^{III}_2O_3(OMe)_6(HOMe)_4(sao)_6(H_2O)_2]$	103	S7
$[Fe^{III}_6Dy^{III}_3(\mu_7\text{-}C_2H_2O_4)(\mu_4\text{-tea})_2(\mu_3\text{-teaH})_4(\mu_2\text{-}N_3)_2(N_3)_6(NO_3)]2EtOH$	65.1	S8
$[(L1)_2Co^{II}_2Gd^{III}]NO_3$	27.4	S9
$Ni^{II}_2Dy^{III}_2(L2)_{10}(bipy)_2$	105	S10

[{$Cu^{II}(dpk)_2$}{$Tb^{III}(hfac)_3$}$_2$]	47	S11
[$Cu^{II}Tb^{III}(L3)_2(NO_3)_3$]	16.6	S12
[$Co^{II}_2Tb^{III}(L4)_2$](NO_3)	14.5	S13
[$Fe^{III}Dy^{III}(L5)_2(NO_3)_4$]	12.9	S14
[$Co^{II}_2Dy^{III}(L1)_2$](NO_3)·2$CHCl_3$·2H_2O	8.0	S15
[$Ni^{II}Dy^{III}(L6)(NO_3)_3$]·2MeOH	7.6	S16
1-Cr-Dy	**~1.4**	**This work**
1-Mn-Dy	**~3.8**	**This work**
1-Fe-Dy	**~2.3**	**This work**
1-Co-Dy	**~2.5**	**This work**

H_2mdea = methyldiethanolamine; $C_2H_2O_4^{4-}$ = tetra anion of 1,1,2,2-tetrahydroxyethane; H_3**L1** = (S)P[N(Me)N = CH-C_6H_3-2-OH-3-OMe]$_3$; **L2** = 3,5-dichlorobenzoic acid; hfac = hexafluoroacetylacetone; **L3** = $MeOC_3H_6NH_2$; **L4** = *N,N′,N″*-tris(2-hydroxy-3-methoxybenzilidene)-2-(aminomethyl)-2-methyl-1,3-propanediamine; **L5** = bis(2-pyridylcarbonylamine); **L6** = *N*,*N*′,*N*″-trimethyl-*N*,*N*″-bis(2-hydroxy-3-methoxy-5-methylbenzyl)diethylene triamine.

Section S3 Additional Figures and Characteristics

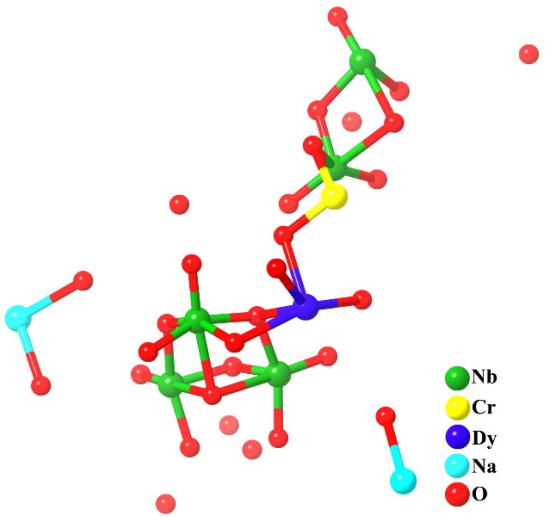

Fig. S1 Asymmetric unit of **1-Cr-Dy**.

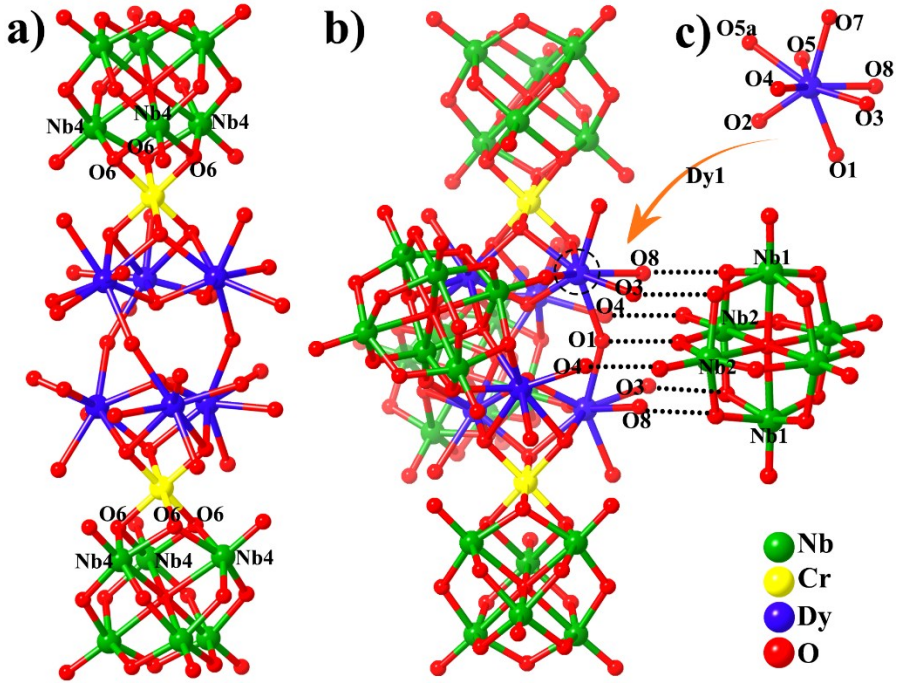

Fig. S2 (a-b) Linkage pattern between $\mathbf{Cr_2Dy_6}$ and $\mathbf{Nb_6}$ on both ends and equatorial position, respectively; (c) the coordination geometry of Dy1.

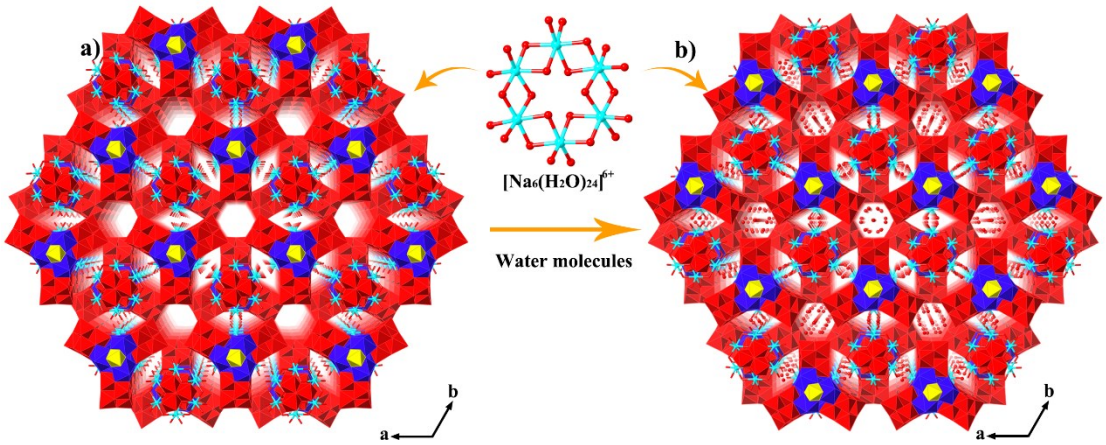

Fig. S3 a) and b) View of the hexagonal close-packed structure of **1-Cr-Dy** along the *c*-axis.

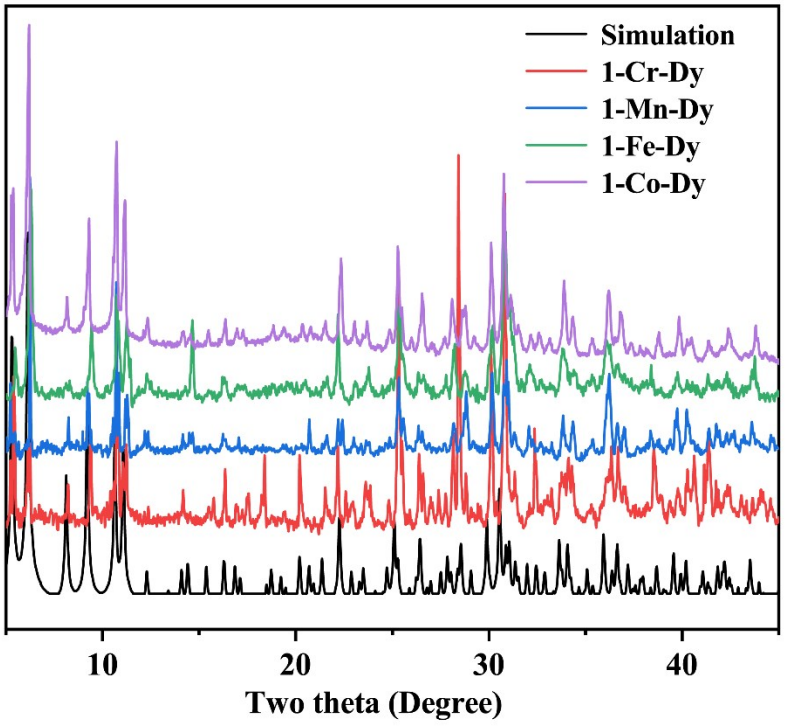

Fig. S4 Simulated and experimental PXRD patterns of **1-TM-Dy.**

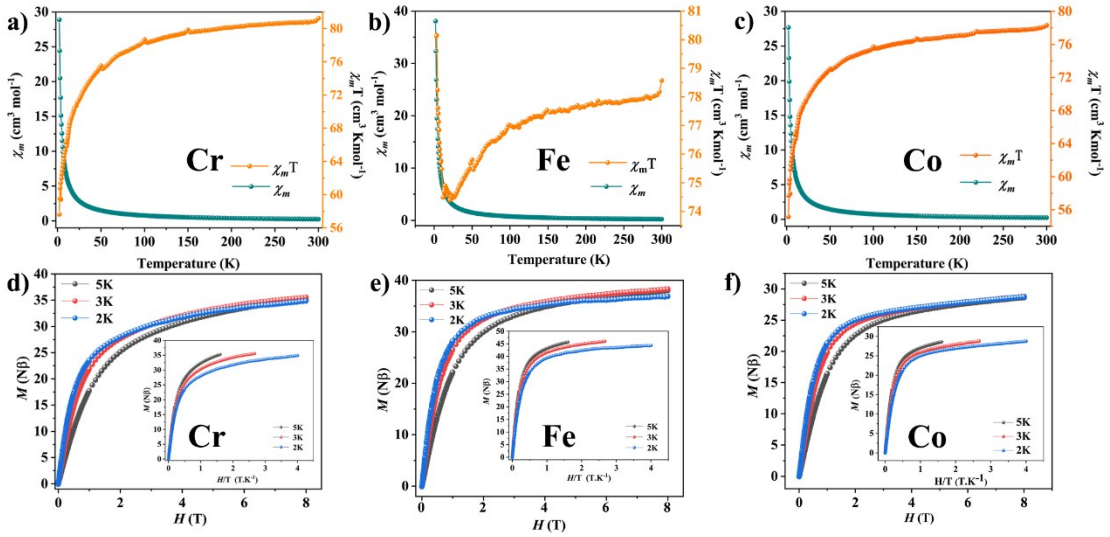

Fig. S5 (a-c) χ_m versus T and χ_mT versus T for **1-Cr-Dy**, **1-Fe-Dy**, and **1-Co-Dy** in the temperature range of 2-300 K; (d-f) the field dependence of magnetization at 2.0 K, 3.0 K and 5.0 K for **1-Cr-Dy**, **1-Fe-Dy**, and **1-Co-Dy**. Inner: (*M*) vs. (*H/T*) plots at 2.0 K, 3.0 K and 5.0 K.

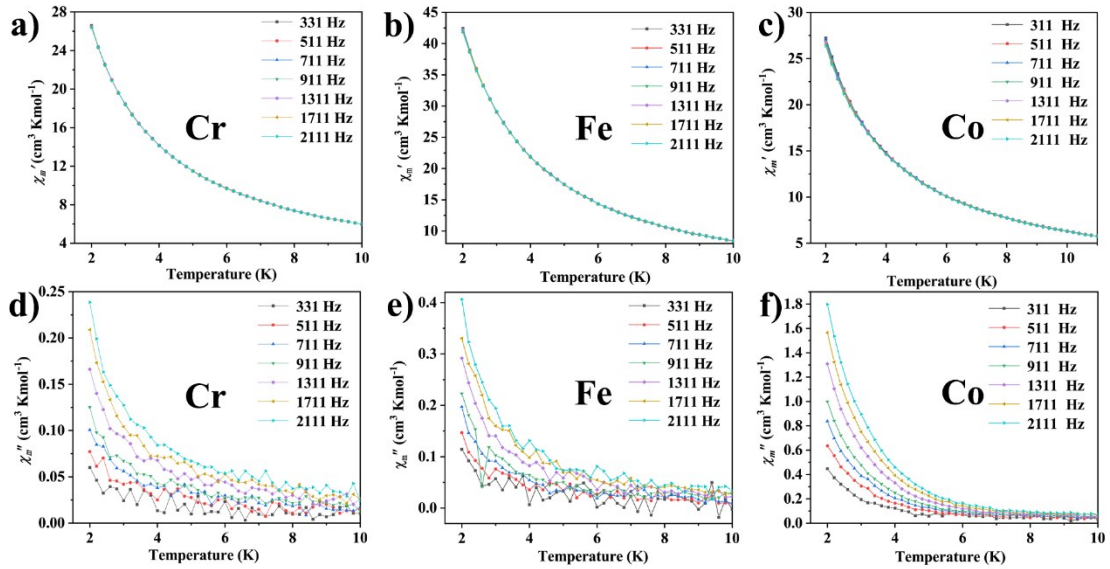

Fig. S6 Temperature-dependent behavior of the in-phase (χ_m') and out-of-phase (χ_m'') of **1-Cr-Dy**, **1-Fe-Dy**, and **1-Co-Dy** in zero static fields at 2-10 K.

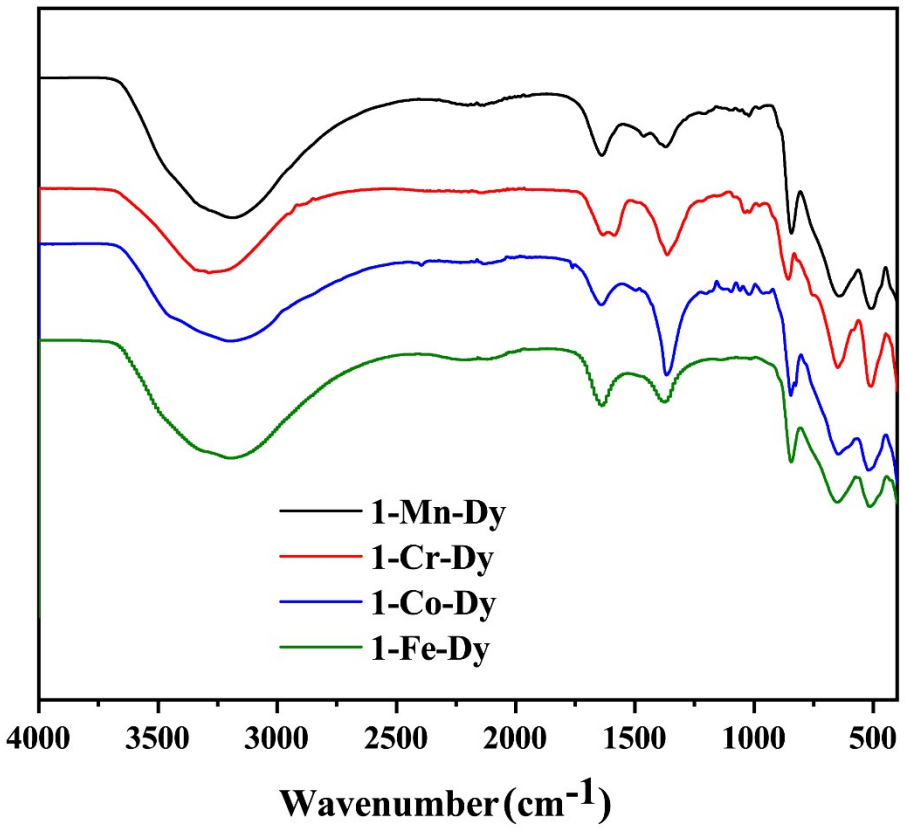

Fig. S7 IR spectra of **1-TM-Dy**.

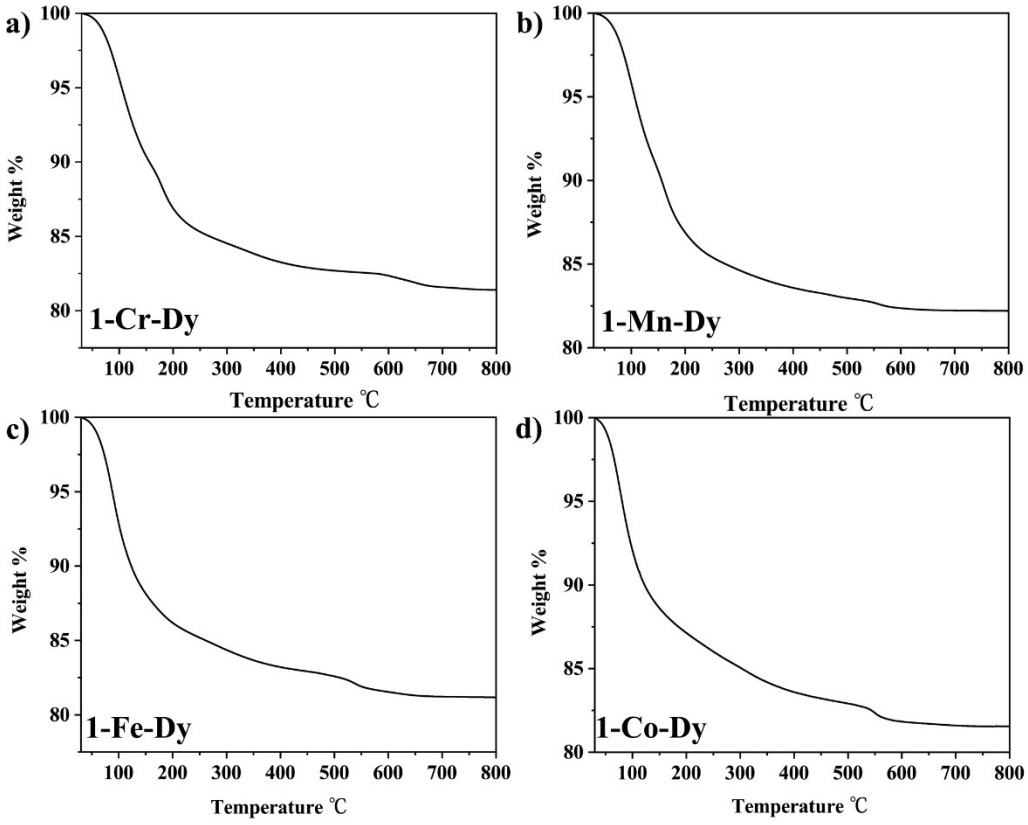

Fig. S8 TGA curves of samples **1-TM-Dy**.

As shown in Fig. S8, all of **1-TM-Dy** experienced a continuous weight loss process in the temperature range of 30 °C to about 550 °C. The first weight-loss stage that occurs when the temperature was within the temperature range of 30 °C to 250 °C should be ascribed to the loss of lattice water molecules. Based on the first weight loss, 56, 57, 57 and 50 lattice water molecules were added for **1-TM-Dy**, TM = Cr, Mn, Fe and Co, respectively.

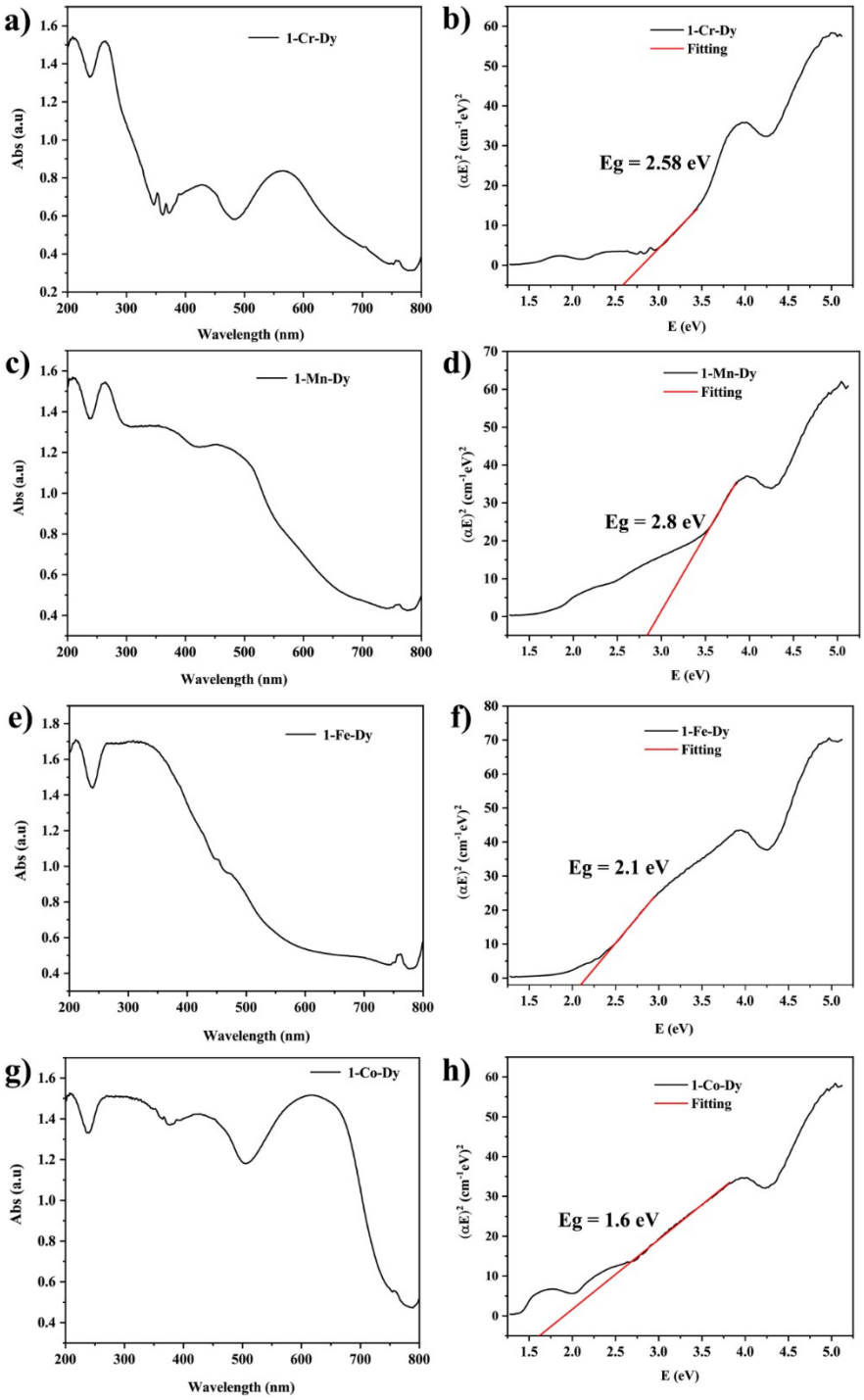

Fig. S9 The UV-Vis absorption spectra and Kubelka-Munk Function vs. energy curves of **1-TM-Dy**.

Section S4: References

S1 Q. Wu, Y. G. Li, Y. H. Wang, E. B. Wang, Z. M. Zhang and R. Clérac, *Inorg. Chem*., 2009, **48**, 1606-1612.

S2 S. H. Chen, V. Mereacre, Z. Y. Zhao,W. W. Zhang, M. S. Zhang and Z. Z. He, *Dalton Trans*., 2018, **47**, 7456-7462.

S3 K. R. Vignesh, R. B.C. Martin, G. Miller, G. Rajaraman, K. S. Murray and S. K. Langley, *Polyhedron*., 2019, **170,** 508-514.

S4 G. Abbas, Y. H. Lan, V. Mereacre, G. Buth, M. T. Sougrati, F. Grandjean, G. J. Long, C. E. Anson and A. K. Powell, *Inorg. Chem.*, 2013, **52**, 11767-11777.

S5 Y. Peng, M. K. Singh, V. Mereacre, C. E. Anson, G. Rajaraman and A. K. Powell, *Chem. Sci***.**, 2019,**10**, 5528-5538.

S6 J. Rinck, G. Novitchi, W. Van den Heuvel, L. Ungur, Y. Lan, W. Wernsdorfer, C. E. Anson, L. F. Chibotaru and A. K. Powell, *Angew. Chem. Int. Ed.*, 2010, **49**, 7583-7587.

S7 M. Hołyńska, D. Premužić, I.-R. Jeon, W. Wernsdorfer, R. Clérac and S. Dehnen, *Chem. Eur. J.*, 2011, **17**, 9605-9610.

S8 S. Schmidt, D. Prodius, V. Mereacre, G. E. Kostakis and A. K. Powell, *Chem. Commun.*, 2013, **49**, 1696-1698.

S9 V. Chandrasekhar, B. M. Pandian, R. Azhakar, J. J. Vittal and R. Clérac, *Inorg. Chem.*, 2007, **46**, 5140-5142.

S10 F. H. Zhao, H. Li, Y. X. Che, J. M. Zheng, V. Vieru, L. F. Chibotaru, F. Grandjean and G. J. Long, *Inorg. Chem.*, 2014, **53**, 9785-9789.

S11 F. Mori, T. Nyui, T. Ishida, T. Nogami, K.-Y. Choi and H. Nojiri, *J. Am. Chem. Soc.*, 2006, **128**, 1440-1449.

S12 T. Kajiwara, M. Nakano, S. Takaishi and M. Yamashita, *Inorg. Chem.*, 2008, **47**, 8604-8606.

S13 T. Yamaguchi, J. P. Costes, Y. Kishima, M. Kojima, Y. Sunatsuki, N. Bréfuel, J. P. Tuchagues, L. Vendier and W. Wernsdorfer, *Inorg. Chem.*, 2010, **49**, 9125-9135.

S14 M. Ferbinteanu, T. Kajiwara, K.-Y. Choi, H. Nojiri, A. Nakamoto, N. Kojima, F. Cimpoesu, Y. Fujimura, S. Takaishi and M. Yamashita, *J. Am. Chem. Soc.*, 2006, **128**, 9008-9009.

S15 V. Chandrasekhar, B.M. Pandian, J.J. Vittal and R. Clérac, *Inorg. Chem.*, 2009, **48**, 1148-1157.

S16 E. Colacio, J. Ruiz-Sanchez, F.J. White and E.K. Brechin, *Inorg. Chem.*, 2011, **50**, 7268-7273.